Catal Lett (2017) 147:2269–2278
DOI 10.1007/s10562-017-2131-4

Catalytic Oxidation of Cyclopentene by O_2 over Pd(II)-SBA-15 Complexes

Lumin Yue[1] · Zhenwei Wang[1] · Lele Bao[1] · Wei Fu[1] · Li Xu[1] · Jun Li[1] · Guanzhong Lu[1]

Received: 14 March 2017 / Accepted: 24 June 2017 / Published online: 6 July 2017

Abstract Novel catalysts with Pd(II)-picolinamide complexes anchored into the channels of mesoporous material SBA-15 were prepared for chemical transformation of cyclopentene, and characterized in details. Spectra of ^{29}Si NMR, ^{13}C NMR and XPS revealed the organic ligands were grafted into the SBA-15 and Pd(II) complexes formed. Spacial diversity of the complexes, especially distances from –C=O to N on pyridyl cycles, may influence electronic distribution of conjugated system and further the catalytic activity. With the help of the newly synthesized catalytic materials, a new heterogeneous oxidation system was developed for selective catalytic transformation of cyclopentene to cyclopentanone with molecular oxygen as the sole oxidant. Analytic results of the reaction mixtures indicated that all catalysts exhibited high activity, while the cat.1 and cat.2 with 2-pyridinecarbonyl or 3-pyridinecarbonyl on the ligands gave better yields of cyclopentanone. 96.2% conversion of cyclopentene and 76.3% yied of cyclopentanone were achieved over the catalyst cat.2 under the conditions of 0.7 MPa O_2, 323 K and 6 h reaction. In addition, the catalysts were also appealing for easy separation and recyclable property.

Graphical Abstract

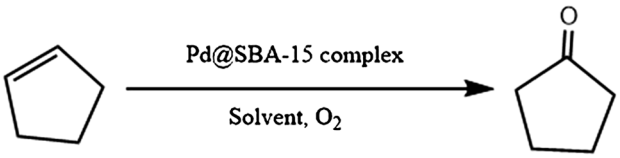

A new heterogeneous reaction system was developed for the catalytic oxidation of cyclopentene to cyclopentanone by molecular oxygen over novel catalysts. The synthesized catalysts are comprised of Pd(II)-picolinamide complexes anchored into the channels of SBA-15. The new system was efficient for the mentioned reaction, and the catalysts were reusable.

Keywords Cyclopentene oxidation · Pd(II)-complexes · Heterogeneous catalysis · Cyclopentanone

1 Introduction

Pd(II)-containing catalysts were widely adopted for the oxidation of terminal alkenes to corresponding ketones [1–4]. The homogeneous palladium catalyst was an effective catalyst for Wacker reaction and the reaction has become an important process in chemical industry. However, it was difficult to separate the homogeneous palladium catalyst from reaction mixture, residual catalyst may contaminated products and reactors.

Ligand modulation of catalyst anchored to supports was an effective method to alleviate separation difficulties [5–8]. Moreover, reusability, high activity, and low metal loading may be achieved by this way. For example, a reusable heterogeneous catalyst with KIT-6-SH ligand, brought about a satisfying recyclability (metal leaching

Electronic supplementary material The online version of this article (doi:10.1007/s10562-017-2131-4) contains supplementary material, which is available to authorized users.

✉ Jun Li
junliecust0967@sina.com

[1] School of Chemical and Environmental Engineering, Shanghai Institute of Technology, Shanghai 201418, People's Republic of China

~0.49 ppm after 8 cycles) and activity (yield: 93%) in the Suzuki–Miyaura reaction [7]. Heterogeneous catalysts with several organic functional groups were attracting more and more attentions [9].

Metals can be anchored to functionalized supporters via coordinating with functional groups. The spatial position of functional groups may change the electronic density distribution around active center and further the catalytic performance. This spatial effect had enormous potential for controlling the heterogeneous reaction, which can be used to synthesize specific target products. The activity vs distance behavior may be qualitatively different. In the case of acid and thiol groups, the catalytic activity for bisphenol synthesis reached the highest when the two groups were as close as possible [10]. Therefore, how to locate these functional groups on ligand compounds was a crucial issue in order to improve the catalytic performance of polyfunctional heterogeneous catalysts.

Mesoporous silica SBA-15 with a large quantity of surface silanol groups can be grafted on by organosilane [10–13]. Silanized mesoporous silica SBA-15 functionalized with a variety of functional groups was widely used as an ideal supporter for immobilizing metal-complexes or metal nanoparticles [14–16]. Although metal-complexes coordinated with the functional groups distributed evenly on the heterogeneous catalyst, the electron density distribution over the ligand groups varied with the anchored sites. Catalytic efficiency increased with enhancing the basicity at the coordination sites or the electron availability of the chelating ring, which accelerated the π-bond formation between metal and olefin [17].

Inspired by above ideas, we have developed novel heterogeneous catalysts for the selective oxidation of cyclopentene in which Pd(II) coordinate with two functional groups. In particular, acylamino and pyridyl were grafted on SBA-15 via two-step surface modification. The activity and stability of the heterogeneous catalysts were investigated in the selective oxidation of cyclopentene by O_2. Three developed catalysts all gave high activity and reusability in the selective oxidation of cyclopentene to cyclopentanone by molecular oxygen.

To the best of our knowledge, this is the first report of cyclopentene oxidation over heterogeneous Pd(II) catalysts with molecular oxygen as the oxidant. The performance of the Pd(II)-complexes is satisfying for more than 96% conversion of the substrate and 76% selectivity to the goal product under favorable conditions. The strategy to immobilize metal ions on a solid support may set a good example for other reactions with transition metal cations as active ingredients of catalysts.

2 Materials and Methods

2.1 Chemicals

All reagents were purchased from Sinopharm in analytical grade without further purification. These reagents are listed as flowing: Tetraethylorthosilicate (TEOS, 99.99%), P123 (average Mn ~5800), HCl (36.0 ~38.0%), ethanol (≥99.8%), 2-picolinate acid (99%), 3-pyridinecarboxylic acid (99.5%), 4-picolinate acid (99%), thionyl chloride (≥99%), dimethylbenzene (≥99.8%), 3-aminopropyltriethoxysilane (≥99.8%), dichloromethane (≥99.5%), acetone (≥99%), palladium chloride (≥99%), cupric chloride (99%), cyclopentene (98%), cyclopentanone (99%), KBr (SP, ≥99%).

2.2 Preparation of Catalysts

2.2.1 Synthesis of SBA-15 (Step I)

SBA-15 was prepared according to the reported process [10–16, 18, 19]. In a typical process, P123 (4 g) was dissolved in HCl solution (120 ml, 2 M) with continuously stirring at 40 °C for 2 h. TEOS (8.5 g, 0.04 mol) was introduced in with stirring for another 24 h at the same temperature. The obtained mixture was transferred into a Teflon-lined autoclave and then hydrothermally kept at 100 °C for 48 h. The suspension was filtrated and washed with ethanol for several times. The filter cake was dried at 100 °C for 3 h and calcined at 550 °C for 6 h in a muffle furnace to obtain SBA-15.

2.2.2 Synthesis of Pyridinecarbonylchloride (Step II)

In a typical process [20], 2-picolinic acid (6.15 g) was dissolved in methylbenzene (70 ml). Thionylchloride (11.9 g) was added into the solution drop wise. The mixture was refluxed at 100 °C for 10–12 h with vigorous stirring under nitrogen atmosphere. Finally, 2-pyridine acyl chloride was obtained after removing the solvent by rotary evaporation. Similarly, 3-pyridine acyl chloride and 4-pyridine acyl chloride was synthesized from 3-picolinic acid and isonicotinoyl chloride, respectively.

2.2.3 Modifying of SBA-15 by Bifunctional Compounds (Step III)

SBA-15 was silanized with aminopropyltriethoxysilane according to the reported method [11, 12]. SBA-15 (2.5 g) reacted with aminopropyltriethoxysilane (5 g) in the mixed solvent of dimethylbenzene (100 ml) and dichloromethane (20 ml) under nitrogen atmosphere for 24 h with vigorously stirring. The obtained suspension

was filtered, washed with ethanol and dried under vacuum at 120 °C for 3 h, marked as SBA-15-R.

SBA-15-R was dispersed with 100 ml dimethylbenzene, followed by the introduction of 2-pyridinecarbonyl chloride (2 g). The mixture was refluxed for 24 h, cooled to room temperature, and filtered with the mixed solvent of 30 ml acetone and 30 ml ethanol for three times. The obtained filter cake dried at 120 °C for 5 h under vacuum, marked as SBA-15-R-2Py (support 1). 3-Pyridinecarbonyl chloride and isonicotinoyl chloride were handled in similar processes, and marked with SBA-15-R-3Py (support 2) and SBA-15-R-4Py (support 3). The amount of immobilized pyridine was determined by elemental analysis.

2.2.4 Immobilization of Pd(II) [or Cu(II)] Onto Modified SBA-15 (Step IV)

The modified SBA-15 reacted with $PdCl_2$ (or $CuCl_2$) in acetone for 72 h. The suspension was filtered and then washed with ethanol and dried at 120 °C for 3 h under vacuum. In this way, target catalysts SBA-15-R-2Py-Pd (cat.1), SBA-15-R-3Py-Pd (cat.2), SBA-15-R-4Py-Pd (cat.3), SBA-15-R-2Py-Cu (sub-cat.1), SBA-15-R-3Py-Cu (sub-cat.2) and SBA-15-R-4Py-Cu (sub-cat.3) were obtained, the processes are presented schematically in Schemes S1, S2 and S3 (Supporting Materials), whereas the final structures of the catalysts are graphically shown in Fig. 1. The loadings of Palladium in the samples was determined by ICP.

2.3 Catalyst Characterization

X-ray diffraction patterns (XRD) were carried out with a Bruker D8 X-ray diffractometer using Cu–K radiation ($\lambda = 0.15405$ nm). Data were collected over the $0.5 \leq 2\theta \leq 6°$ region. Scanning electron microscopy (SEM) images were acquired using BRUKERS-3400N. Transmission electron microscopy (TEM) micrographs were obtained with a Tecnai G^2 20 (FEI Company). Specific surface area measurement and porosity analysis were performed using N_2 adsorption isotherms (Micromeritics, ASAP 2010 MICROPORE dry Analyzer). UV–Visible diffuse reflectance spectra were measured using UV-3600 (Shimadzu) between 200 and 600 nm. FT-IR spectra were recorded using NICOLET iZ10 with 64 scans between 400 and 4000 cm^{-1} [18, 19, 21] with KBr as the standard. Elemental analysis (%C and %N) were analyzed using Elementar Vario EL III. The loadings of Palladium in the samples were determined by ICP-AES (Perkinelmer, Optima 7000 DV). Thermogravimetric analysis was performed using a Netzsch thermoanalyzer STA 449F3 at a heating rate of 10 °C/min in air.

2.4 Activity Test of the Catalyst

Cyclopentene oxidation was carried out in a Teflon-lined stainless steel reactor (100 ml) equipped with a magnetic stirrer. In a typical reaction, the reactor was flushed with molecular oxygen, then cyclopentene (4.5 g) was mixed with solvent (6 g), water (0.3 g), O_2 (0.2 MPa), cat. (0.1 g) and sub-cat. (0.3 g). Pure molecular oxygen was recharged into the reactor to 0.7 MPa when reaction temperature 50 °C was attained. After reaction, the mixture of the reactant and products was cooled down to room temperature and centrifuged to separate the catalyst. The products were analyzed by HPLC (High Performance Liquid Chromatography, Agilent 1100).

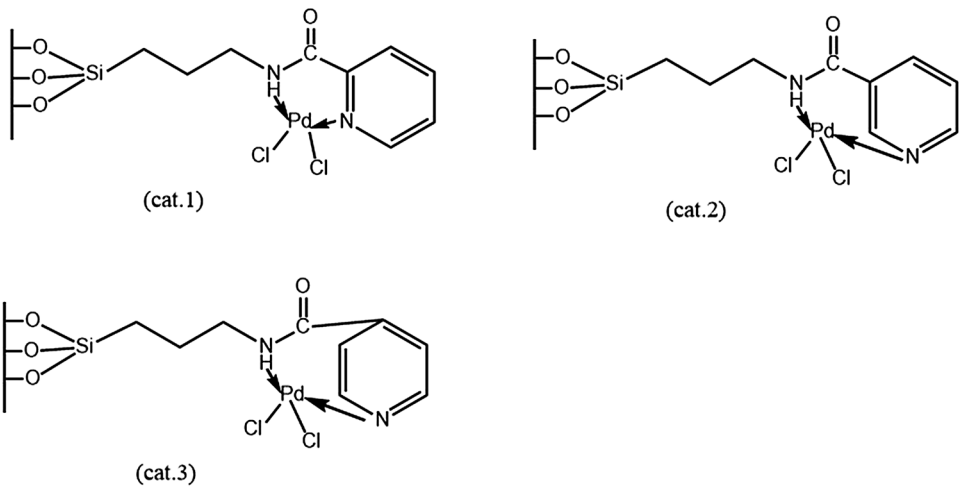

Fig. 1 Structures of the catalysts

2.5 Recycling Studies

Recycling studies were also carried out with cyclopentene oxidation. The reaction was performed under following conditions: cyclopentene (4.5 g), ethanol (6 g), water (0.3 g), cat. (0.1 g, Pd-0.04 mmol), sub-cat. (0.3 g), reaction temperature 50 °C, O_2 pressure 0.7 MPa and reaction time 6 h. The catalyst was filtered, washed with ethanol and dried under vacuum at 100 °C for 3 h. Then it was reused in the next run. The loadings of Pd in the catalyst were determined using ICP before and after each run.

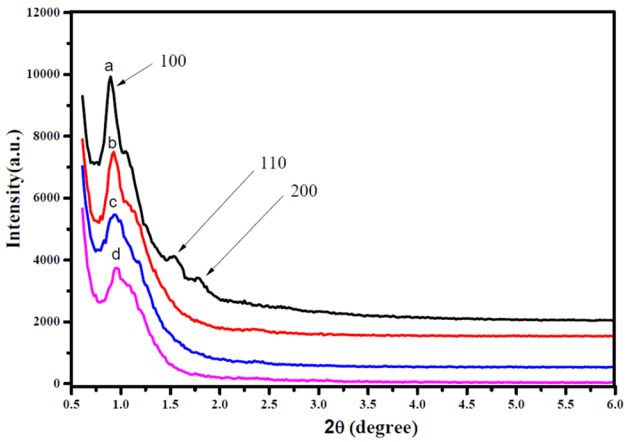

Fig. 2 Small-angle XRD patterns of SBA-15 (*a*), cat.1 (*b*), cat.2 (*c*) and cat.3 (*d*)

3 Results and Discussion

3.1 Characterization of Pd-Catalysts

Figure 2 shows small-angle XRD patterns of SBA-15 and other three samples cat.1, cat.2 and cat.3. The main diffraction peaks (100) for the samples cat.1, cat.2 and cat.3 are similar to that of the SBA-15, indicating the long-range ordered mesoporous structure of the SBA-15 was basically retained after modification [22, 23].

SEM images (Fig. 3) reveal that all samples keep wheat-like macrostructures identical to that of SBA-15 [24]. Both the uniformity of the mesopore size and the existence of mesopore channels of these catalysts are confirmed by TEM image (Fig. 3e). The TEM image reveals the absence of any palladium particles inside the channels, indicating the functionalization and loading steps have no negative impact on the ordered mesoporous structure of the catalysts.

Table 1 gives the results for N_2 adsorption–desorption, including pore diameters (D_{BJH}), BET surface area (S_{BET}) and total pore volumes (V_{total}) of these catalysts. The type IV profile with a sharp hysteresis loop indicates that all catalysts have the highly ordered mesoporous structure, as presented in Figure S1 (Supporting Materials). Nitrogen adsorption–desorption studies demonstrates that modification on SBA-15 channel surface brings about a significant decrease of S_{BET}, D_{BJH} and V_{total}. The mesoporous construction is still maintained at the same time, as is confirmed with SEM results mentioned above. The presence of Pd in functionalized mesoporous SBA-15 catalyst was quantified by ICP, and the presence of C and N were also confirmed by Elemental Analysis.

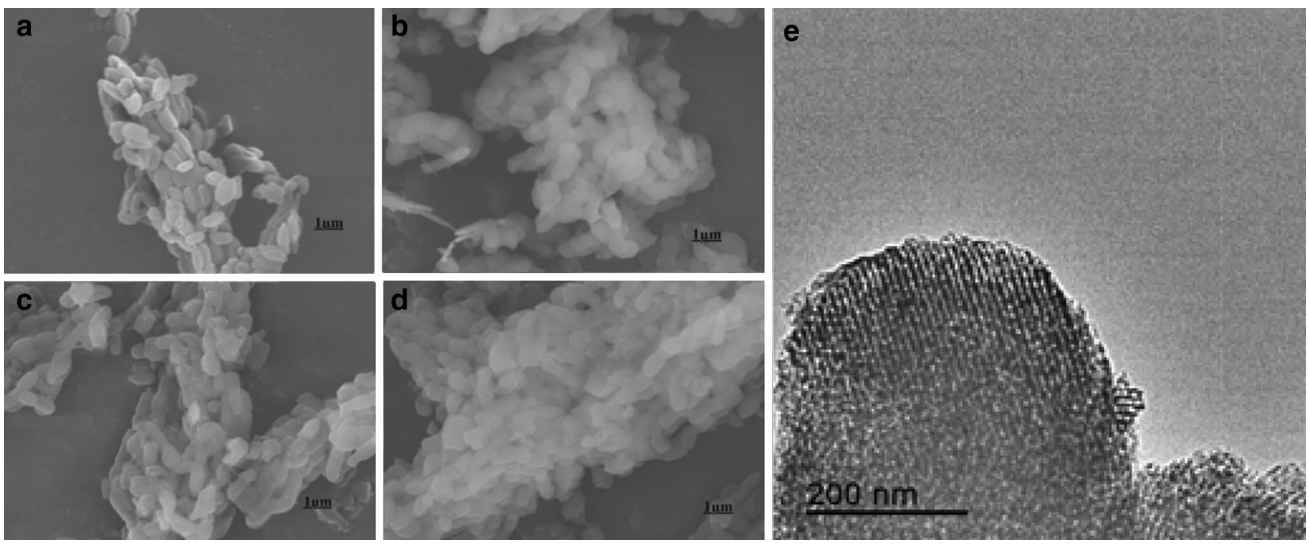

Fig. 3 SEM images of samples: **a** SBA-15, **b** cat.1, **c** cat.2, **d** cat.3; **e** TEM image of cat.2

Table 1 Results of the N_2 adsorption–desorption measurement and elemental analysis

Sample	S_{BET} ($m^2\ g^{-1}$)	V_{total} ($cm^3\ g^{-1}$)	D_{BJT} (nm)	C (wt%)	N (wt%)	Pd[a] (wt%)
SBA-15	409.18	0.97	8.16	–	–	–
Support 1	309.93	0.55	6.14	14.3	3.6	–
Cat.1	286.19	0.50	6.12	–	–	4.82
Support 2	271.76	0.53	7.00	13.6	3.5	–
Cat.2	266.98	0.49	6.48	–	–	4.76
Support 3	255.95	0.48	6.64	14.6	3.6	–
Cat.3	239.25	0.46	6.64	–	–	4.72

[a]The loadings of Pd in the samples were determined by ICP

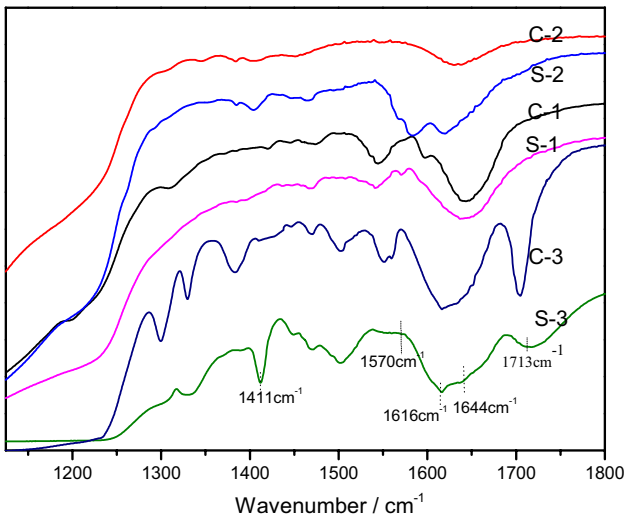

Fig. 4 FT-IR spectra of the supports 1, 2 and 3 (*S-1, S-2* and *S-3*) and catalysts 1, 2 and 3 (*C-1, C-2* and *C-3*)

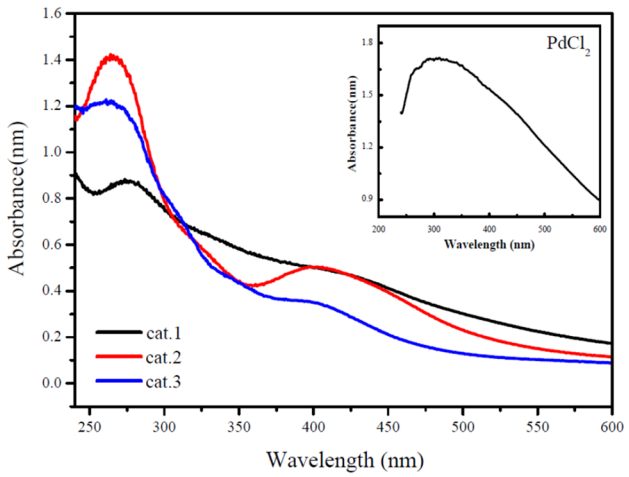

Fig. 5 Solid-state diffuse-reflectance UV/visible spectrum of catalysts and $PdCl_2$ (*inset*)

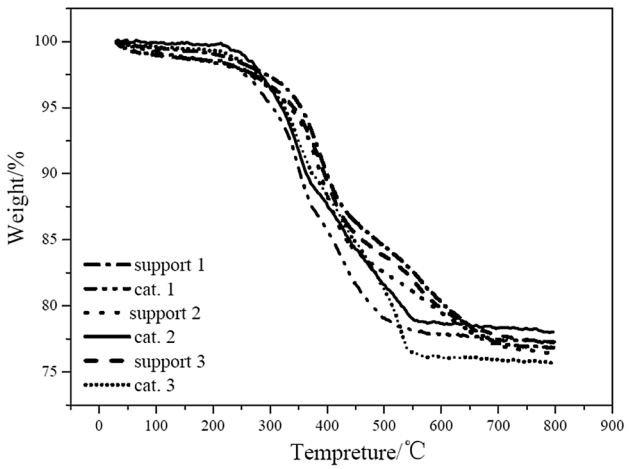

Fig. 6 Thermogravimetric analysis results of different samples

Figure 4 shows the FT-IR spectra for the supports and catalysts in the range of 1150–1800 cm^{-1}. The bands centered at 1659, 1644 and 1713 cm^{-1} for the lines of support 1, support 2, support 3 are assigned to the vibrations of carbonyls in the supports [14, 18], the band peaks shifted to 1606, 1603 and 1647 cm^{-1} respectively after Pd-ligand complexes were formed, corresponding to the vibrations of carbonyls on the acylaminos for cat.1, cat.2 and cat.3, indicating O on the acylaminos may be involved in the coordination of Pd ions and the ligands. The bands in the range of 1620–1400 cm^{-1} represent the vibration absorptions of the bonds C=C, and C=O in the pyridine rings [14, 24]. The absorption peaks centered at 1591, 1597 and 1616 cm^{-1} for the supports shifted to 1570, 1580 and 1577 cm^{-1} respectively for the corresponding catalysts, evidencing N in the the pyridine rings taking part in the formation of the Pd-ligand complexes. The absorption peaks centered at 1243, 1242, and 1247 cm^{-1} for support 1, support 2 and support 3 are ascribed to vibration absorptions of the bonds N–H on the acylamino$_s$ of the ligands [21, 24], which shift to 1235, 1232 and 1237 cm^{-1} in turn owing to coordinations of N in the second amides with Pd ions.

Generally speaking, characteristic peaks of the stretching bands of the functional groups involved in coordination

move to lower wavelength [6, 14, 24]. The donor atoms are the nitrogen atoms in pyridine rings and the nitrogen atoms of amides. C=N peak moving to lower wave number means the formation of metal–ligand bonds [14].

The larger shift of C=N stretching band means stronger bonding between Pd(II) and organic ligand. Shifting to low wave number of C=O peak is probably caused by the pyridine ring. Molecular structure of N-(3-(triethoxysilyl) propyl)picolonicamide (TPP) is not planar, and there is an angle between pyridyl ring and –C–N bond [25]. So there has something different of the coordination between Pd(II) and the donors for these three catalysts. Stable Pd(II)-complexes of five-membered cycles are to be formed easily with cat.1 owing to the favorable locations of the coordinating atoms on the ligands as shown in Schemes. For cat. 2 and cat. 3, palladium cations also coordinate with two N atoms on the respective ligands, the structures and performances of the complexes may impacted by the conjugated π bonds on the pyridyl rings, especially for the cat. 3.

These developed catalysts are detected by the solid-state diffuse UV/visible spectrum, as shown in Fig. 5. Absorbance bands appear around near 265 and 400 nm, while the untreated precursor material ($PdCl_2$) shows no absorbance band around similar regions (Fig. 5, inset). It is supposed that these bands near 265 nm (cat.2, cat.3) and 275 nm (cat.1) are the characteristic absorption of pyridine derivatives and the band near 400 nm is the characteristic absorption of coordinated Pd(II) which initially locates nearly

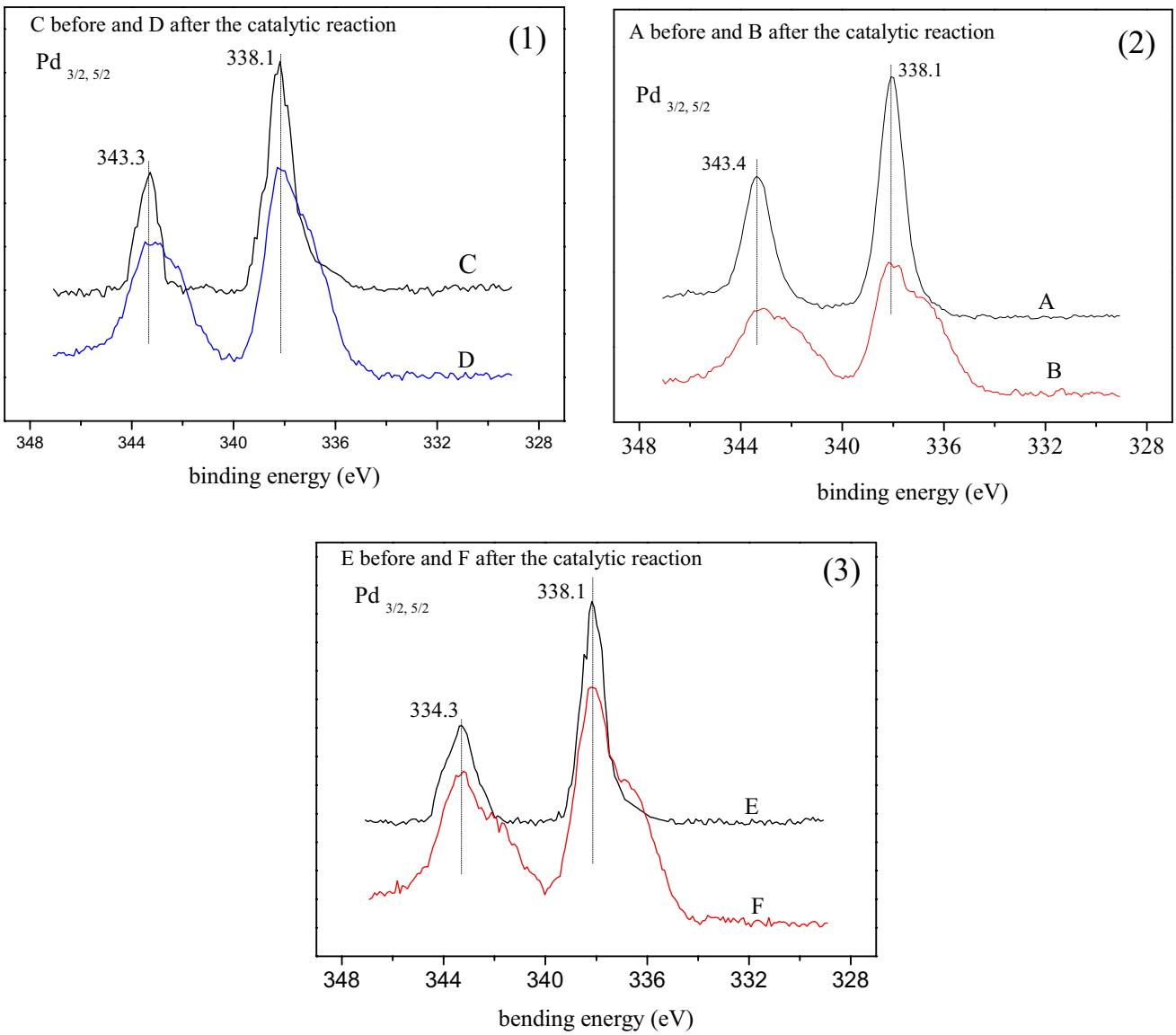

Fig. 7 XPS spectra of cat.1 (**1**), cat.2 (**2**) and cat.3 (**3**) before and after use

at 300 nm in free-state. The corresponding absorption of Pd(II) shifts to long wavelength which is also an indication of the formation of metal–ligand bonds.

There are several reports in literature about changes occurring in the thermal degradation of metal complexation as well as chemical modified catalysts. For example, the correlations of thermal degradation properties of a series of metal complexes has been reported [26]. The decrease in the observed thermal stability is intimately related to the specific type of metal complex. Figure 6 shows thermogravimetric analysis results for picolinamide-modified SBA-15 and their metal complexes. All the samples exhibit two stage degradation. Supports give the first degradation temperature range between 380 and 410 °C and the second degradation range between 540 and 590 °C. In contrast, catalysts show the first degradation range of 330–370 °C and the second degradation range of 400–430 °C. Obviously, the thermal stability at higher temperature range decreases after metal coordination although all catalysts keep steady before 200 °C.

X-ray photoelectron spectroscopy (XPS) measurements were carried out for cat.2 before and after the oxidation reaction. Pd $3d_{3/2,\ 5/2}$ XPS spectra are shown in Fig. 7(1–3). For Fig. 7(2)—A, a single chemical state is present with Pd $3d_{3/2}$ and $3d_{5/2}$ peaks at binding energies of 343.4 and 338.1 eV, respectively. Pd $3d_{5/2}$ 338.1 eV for the cat.2 is similar to the published data with $Pd(OAc)_2$ supported on PMO [27], indicating the presence of Pd(II) species in the cat.2. The binding energy of 338.1 eV is lower than that for $PdCl_2$ (338.5 eV) [28], indicating that there is an electronic interaction between Pd (II) and the ligands for the cat2. In Fig. 7(2)—B, besides the peaks 343.4 and 338.1 eV, shoulders appear to the right of the main peaks respectively, evidencing there may be new state of Pd species upon reaction, which is presumably ascribed to Pd particles formed during the reaction. For cat.1, and cat.3, XPS spectra are analogous to that of the cat.2, indication the three catalysts underwent similar processes and displayed like behaviors.

The presence of organic functional groups was further confirmed by NMR spectroscopy. ^{29}Si NMR spectra of SBA-15 and the cat.2 are shown in Fig. 8, distinct resonances can be observed for the siloxane [$Q^n = Si–(OSi)_n–(OH)_{4-n}$, n = 2–4; Q^2 at −93, Q^4 at −111 ppm and Q^3 at −103 ppm] and organosiloxane [$T^m = RSi(OSi)_m–(OH)_{3-m}$, m = 1–3; T^3 at −68 ppm and T^2 at −60 ppm] species [29, 30]. The appearance of T^3 and T^2 peaks for cat.2 confirms a strong covalent linkage between the organic groups and the silica surface.

The obtained materials were also characterized by means of solid state ^{13}C NMR spectroscopy. The peak assignments are mentioned in Fig. 9, the strong signals at 13.7, 25.5 and 47.1 ppm are attributed to the methylene carbons (C_1, C_2 and C_3) respectively. The signal at 175.3 ppm

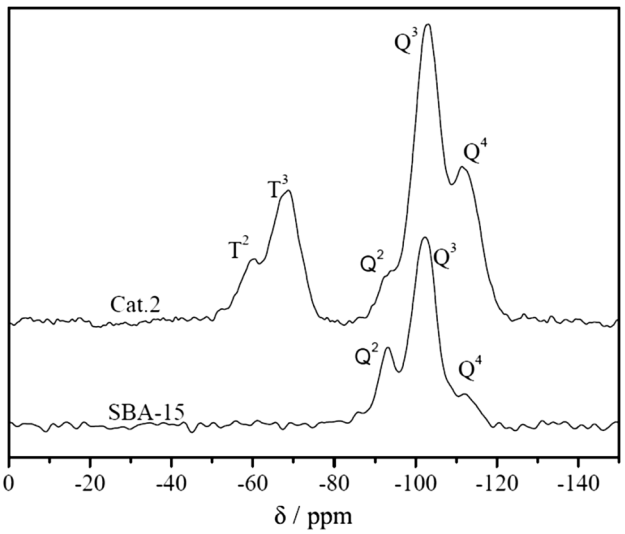

Fig. 8 ^{29}Si NMR spectra of SBA-15 and the cat.2

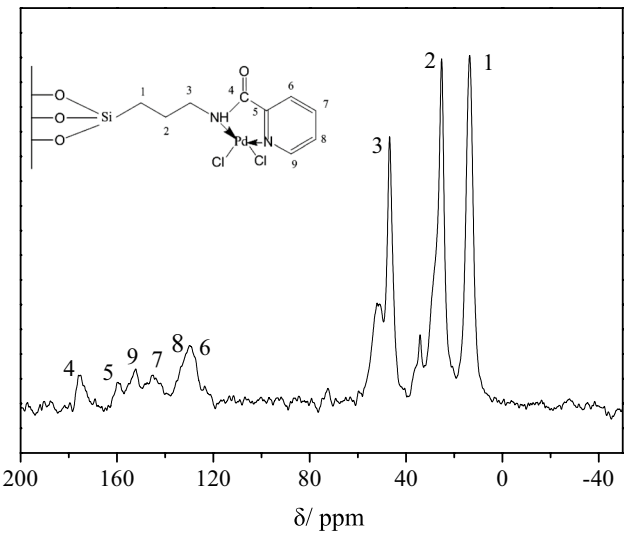

Fig. 9 ^{13}C NMR spectrum of the cat.2

dramatically decreases in height indicating strong chemical bonding between the Pd and amide group, which in turn effects the peak of C_4 attached to the amide group [31].

3.2 Catalytic Performance of the Pd(II) Complexes for the Title Reaction

The catalyst activity are tested using cyclopentene oxidation (Scheme 1). The date presented in Table 2 indicates that solvent, reaction temperature, catalyst loading and O_2 pressure are critical for the reaction outcomes.

It is well known that the nature of solvent plays a very important role in the catalytic reactions carried out in liquid

phase. To study the influence of solvent nature, the oxidation of cyclopentene with oxygen using cat.2 as catalyst, are carried out at 50 °C and 0.7 MPa O_2 using ethanol, acetonitrile, dimethyl benzene, and polyethylene glycol as solvents respectively. Table 2 (entry 1–4) shows the cyclopentene conversion for all the solvents used. The activity order for these four solvents, acetonitrile > ethanol > polyethylene glycol > dimethylbenzene, are observed. However, the selectivity for cyclopentone with acetonitrile solvent is lower than ethanol solvent. Ethanol are selected in the following reactions.

The effect of O_2 pressure on the reaction is investigated (Table 2, entry 1, entries 14–17). As listed in Table 2, 0.7 MPa is the best O_2 pressure for the reaction with high yield.

The effects of temperature on the reaction are examined. The obvious improvement in the conversion (96.2%) is achieved for the reaction at 50 °C (Table 2, entry 1, entries 10–13).

The influences of catalyst loading are also investigated. The best result is obtained with 0.7 mol‰ (the molar ratio of Pd: cyclopentene) of catalyst (Table 2, entries 1, 5–9).

Finally, with a reliable set of conditions in hand, cat.1 and cat.3 were investigated in the optimal conditions (50 °C, 0.7 MPa O_2, ethanol solvent) when cat.2 was used for the same reaction. The results show the yield of cat.3 is lower compared to those of the cat.1 and cat.2. The inferior

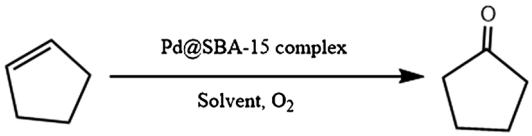

Scheme 1 Oxidation of cyclopentene to cyclopentone

Table 3 Effect of reaction time on cyclopentene oxidation over cat.2

Catalyst	Reaction time/h	Conversion/%	Selectivity/%	Yield/%
Cat.2	2	61.45	67.2	41.336
Cat.2	4	86.57	66.9	57.921
Cat.2	6	96.24	79.04	76.10
Cat.2	8	99.29	71.02	70.52
Cat.2	10	99.89	67.89	67.82

Reaction condition: cyclopentene 4.543 g, ethanol 6 g, water 0.3 g, 50 °C, 0.7 MPa O_2, Cat. 0.1 g

Table 2 Results of cyclopentene oxidation over the developed catalysts

Entry	Cat.	Cat (mol‰)[a]	Solvent	T(℃)	P_{O2} (MPa)	Con. (%)	Yields (%)
1	Cat.2	0.7	Ethanol	50	0.7	96.2	76.3
2	Cat.2	0.7	Acetonitrile	50	0.7	97.8	52.3
3	Cat.2	0.7	Dimethyl benzene	50	0.7	48.8	27.0
4	Cat.2	0.7	Polyethylene glycol	50	0.7	61.7	45.3
5	Cat.2	4	Ethanol	50	0.7	98.8	55.7
6	Cat.2	2	Ethanol	50	0.7	98.3	66.8
7	Cat.2	1.3	Ethanol	50	0.7	97.6	69.2
8	Cat.2	1	Ethanol	50	0.7	97.5	71.4
9	Cat.2	0.5	Ethanol	50	0.7	89.2	55.1
10	Cat.2	0.7	Ethanol	30	0.7	49.3	20.6
11	Cat.2	0.7	Ethanol	40	0.7	78.3	46.2
12	Cat.2	0.7	Ethanol	60	0.7	95.4	69.6
13	Cat.2	0.7	Ethanol	70	0.7	90.6	58.6
14	Cat.2	0.7	Ethanol	50	0.3	84.1	45.7
15	Cat.2	0.7	Ethanol	50	0.5	89.5	64.2
16	Cat.2	0.7	Ethanol	50	1.0	99.3	71.3
17	Cat.2	0.7	Ethanol	50	1.5	99.8	67.2
18	Cat.1	0.7	Ethanol	50	0.7	95.9	75.1
19	Cat.3	0.7	Ethanol	50	0.7	95.1	65.6
20[b]	Pd^0–S	0.7	Ethanol	50	0.7	0	–

Reaction condition: cyclopentene (4.543 g, 0.067 mol), solvent 6 g, water 0.3 g, reaction time 6 h

[a]Molar ratio of Pd: cyclopentene

[b]Pd^0–S denotes a catalyst Pd^0-SBA-15 prepared using incipient wetness impregnation with $PdCl_2$ as the source of palladium and SBA-15 as the support followed by hydrogen reduction

Table 4 Recycle performance of the developed catalysts

Catalysts	Yield[a]				Pd (wt%)[b]	
	Run 1	Run 2	Run 3	Run 4	Fresh	Fourth run
Cat.1	75.1	70.3	64.9	61.3	4.82	4.28
Cat.2	76.1	71.8	71.1	69.7	4.76	4.43
Cat.3	65.6	60.7	58.9	56.8	4.72	4.25

Reaction condition: Cyclopentene (4.543 g, 0.067 mol), Ethanol 6 g, Water 0.3 g, 50 °C, 0.7 MPa O_2, Cat.2 0.1 g, Sub-cat.2 0.3 g, reaction time 6 h

[a]Yield of cyclopentanone (%)

[b]Loadings of Pd in fresh and the used catalysts were determined by ICP analysis

yield with cat.3 may be attributed to the unfavorable spacial structure of this Pd(II) complex.

The diverse performances of the cat.1and cat.2 and cat.3 for the selective oxidation of cyclopentene may be attributed to the different structures of the three Pd(II) complexes stemming from three distinct ligands which were initially formed by 2-pyridinecarbonyl chloride, 3-pyridinecarbonyl chloride and 4-pyridinecarbonyl chloride respectively. Spacial structures of the complexes may be related to the steric hindrance or the electron density of Pd(II) in the complex. For cat.3, conjugated π electrons in the pyridyl rings may have important impacts on the performance of the catalyst leading to the lower selectivity in the goal product compared to the other two catalysts. Pd nanoparticles supported on mesoporous material SBA-15 (denoted as Pd^0–S in the Table 2) did not catalyze the talked reaction efficiently as shown in the above Table 2.

Results of the oxidation reaction are influenced by reaction time. Conversion of the cyclopentene increased with reaction time, while the highest selectivity to the goal product appeared after 6 h reaction leading to the best yield of cyclopentenone. Too long reaction time resulted in poor yields of the goal product as shown in Table 3.

3.3 Catalyst Reusability

Reusability is also a virtual feature for supported catalysts because of leaching of metal species during reaction [6, 16, 32, 33]. The Pd leaching and reusability results of these developed catalysts are summarized in Table 4. Cat.2 shows the best performance on Pd leaching and catalyst reusability than the other two. Pd-leaching of these supported catalysts are all very little after four runs compared with the result of heterogeneous catalysts reported [32, 34] (the leaching of the active metals anchored in mesoporous materials for the Heck Reactions were up to 30.1 and 1.0% respectively after four recycles). Hence, the heterogeneous catalysts shown in this paper can be used for several times without major change in the activity. It can be deduced that the coordinate bonds formed in these three catalysts are relatively strong and the formation rate of the Pd(0) in the circulation of Pd(II)–Pd(0)–Pd(II) can be faster than the aggregation of Pd(0).

4 Conclusions

Selective catalytic oxidation of cyclopentene was successfully implemented with molecular oxygen as the sole oxidant and Pd(II)-Picolinamide Complexes as catalysts in a heterogeneous reaction system. The catalysts were effective for the aforementioned reaction with high yields of the goal product. The synthesized Pd-complex catalysts can be easily recovered by filtration. In other words, the catalytic oxidation system is environmentally friendly. Furthermore, a good yield was obtained even after the catalyst was reused for many times. More work is necessary to achieve a better understanding about the effects of the ligand structures on the final outcomes of the oxidation reaction.

Acknowledgements The authors gratefully acknowledge the financial support of Consortium Plan Project of Shanghai (LM201411), the support of Shanghai Institute of Technology, and the constant support and advice from the Applied Catalysis Group.

References

1. Takehira K, Hayakawa T, Orita H et al (1989) J Mol Catal 53:15–21
2. Takehira K, Oh IH, Hayakawa T et al (1989) J Mol Catal 53:105–109
3. Takehira K, Orita H, Oh IH et al (1987) J Mol Catal 42:247–255
4. Silva AD, Patitucci ML, Bizzo HR et al (2002) Catal Comm 3:435–440
5. Kishi A, Higashino T, Sakaguchi S et al (2000) Tetrahedron Lett 41:99–102
6. Gruber-Woelfler H, Radaschitz PF, Feenstra PW et al (2012) J Catal 286:30–40
7. MacQuarrie S, Nohair B, Horton JH et al (2009) J Phy Chem C 114:57–64
8. Polshettiwar V, Molnár Á (2007) Tetrahedron Lett 63:6949–6976
9. Bass JD, Katz A (2006) Chem Mater 18:1611–1620

10. Margelefsky EL, Zeidan RK, Dufaud V et al (2007) JACS 129:13691–13697
11. Margolese D, Melero JA, Christiansen SC et al (2000) Chem Mater 12:2448–2459
12. Kang T, Park Y, Choi K et al (2004) J Mater Chem, 14:1043–1049
13. Corriu RJP, Lancelle-Beltran E, Mehdi A et al (2002) J Mater Chem 12:1355–1362
14. Paul S, Clark JH (2004) J Mol Catal A 215:107–111
15. Bedford RB, Singh UG, Walton RI et al (2005) Chem Mater 17:701–707
16. Karimi B, Abedi S, Clark JH et al (2006) Angew Chem Inter Ed 45:4776–4779
17. Nair VA, Suni MM, Sreekumar K (2002) J Chem Sci 114:481–486
18. Gao J, Wang L, Liu X et al (2008) J Mol Catal 22:117–122
19. Webb JD, MacQuarrie S, McEleney K et al (2007) J Catal 252:97–109
20. Sayar O, Zhad HRLZ, Sadeghi O et al (2012) Biol Trace Elem Res 150:403–410
21. Parvulescu V, Mureseanu M, Reiss A (2010) Rev Roum Chim 55:1001–1008
22. Veisi H, Hamelian M, Hemmati S (2014) J Mol Catal A 395:25–33
23. Roy S, Chatterjee T, Pramanik M et al (2014) J Mol Catal A 386:78–85
24. Komura K, Nakamura H, Sugi Y (2008) J Mol Catal A 293:72–78
25. Zheng ZN, Lee SW (2014) Polyhedron 69:197–204
26. Trimukhe KD, Varma A (2009) J Carbohyd Polym 75:63–70
27. Parijat Borah, Yanli Zhao (2014) J Catal 318:43–52
28. Chen J, Tang J, Hu C, Wang J, Chin J (2009) J Inorg Chem 25:147–153
29. Shylesh S, Wagner A, Seifert A, Ernst S, Thiel WR Chem Eur J 15(2009) 7052–7062
30. D. Margolese, J. A. Melero, S. C. Christiansen, B. F. Chmelka and G. D. Stucky, Chem. Mater., 12(2000) 2448–2459
31. Wei F, Yue L, Duan X, Jun Li, Lu G (2016) Green Chem 18:6136–6142
32. Zhao F, Bhanage BM, Shirai M et al (2000) Chem A Eur J 6:843–848
33. Ghorbani-Vaghei R, Hemmati S, Veisi H (2014) J Mol Catal A 393:240–247
34. Yang H, Zhang G, Hong X et al (2004) J Mol Catal A 210:143–148